PAMELA, ATIC AND DARK MATTER, OR: SEEING DARK MATTER IN COSMIC RAYS?

MARCO CIRELLI
Institut de Physique Théorique, CNRS, URA 2306 & CEA/Saclay
F-91191 Gif-sur-Yvette, France
E-mail: marco.cirelli@cea.fr

ABSTRACT

Dark Matter constitutes more that 80% of the total amount of matter in the Universe, yet almost nothing is known about its nature. A powerful investigation technique is that of searching for the products of annihilations of Dark Matter particles in the galactic halo, on top of the ordinary cosmic rays. Recent data from the PAMELA satellite and a few balloon experiment have reported unexpected excesses in the measured fluxes of cosmic rays. Are these the first direct evidences for Dark Matter? If yes, which DM models and candidates can explain these anomalies and what do they imply for future searches?
[Report number: SACLAY-T09/045]

1. Introduction

While compelling evidence for the existence of Dark Matter (DM) now comes from a number of astrophysical and cosmological probes (such as galaxy rotation curves, weak lensing measurements and the precise data from the Cosmic Microwave Background observations and the Large Scale Structure surveys of the Universe [1]), no explicit detection has been confirmed yet. The indirect detection strategy relies on the possibility of seeing signals of the presence of DM in terms of the final products ($e^{\pm}$, p, d, γ, $\nu \ldots$) of DM annihilations in the galactic halo, on top of the ordinary cosmic rays.

The recent positive results from a number of indirect detection experiments have suggested the possibility that indeed such a signal has been seen. In particular, the signals point to an excess of electrons and positrons.

- Data from the PAMELA satellite show a steep increase in the energy spectrum of the positron fraction $e^+/(e^+ + e^-)$ above 10 GeV up to 100 GeV [3], compatibly with previous less certain hints from HEAT [4] and AMS-01 [5].
- Data from PAMELA also show no excess in the $\bar{p}/p$ energy spectrum [6] compared with the predicted background.
- The balloon experiments ATIC-2 [7] and PPB-BETS [8] report the presence of a peak in the $e^+ + e^-$ energy spectrum at around 500-800 GeV.
- The HESS telescope has also reported the measurement [10] of the $e^+ + e^-$ energy spectrum above energies of 600 GeV up to a few TeV: the data points show a

steepening of the spectrum which is compatible both with the ATIC peak (which cannot however be fully tested) and with a power law with index -3.05 ± 0.02 and a cutoff at $\approx$2 TeV.

In this presentation I will try to answer the following questions:

- Which characteristics must a Dark Matter candidate have in order to fit the above data?
- What are the constraints from other observations (mainly of photons from the Galactic Center region)?
- As a consequence, which conclusions can be drawn on the Dark Matter interpretation of the data?

The discussion in based on Ref. [11] and Ref. [12].

2. Indirect Dark Matter searches

Indirect searches are one of the most promising ways to detect Dark Matter. DM particles in the galactic halo are expected to annihilate and produce fluxes of cosmic rays that propagate through the galaxy and reach the Earth. Their energy spectra carry important information on the nature of the DM particle (mass and primary annihilation channels). Many experiments are searching for signatures of DM annihilations in the fluxes of γ rays, positrons and antiprotons. We here briefly review the procedures that allow to precisely compute the spectra of these species from DM galactic annihilations, and their associated uncertainty.

2.1. Dark Matter distribution in the Milky Way

As a first point, we need to specify the way the Dark Matter particles (the source of the fluxes searched for) are distributed in the galaxy. The density profile, denoted as $\rho(r)$ as a function of the distance r from the galactic center (assuming spherical symmetry) is computed on the basis of the results of numerical simulations, and several choices are possible. The somehow benchmark-status Navarro, Frenk and White (NFW) profile [18] is given by

$$\rho_{\rm NFW}(r) = \frac{\rho_s}{\frac{r}{r_s}\left(1+\frac{r}{r_s}\right)^2}\,. \tag{1}$$

More recently, Ref. [19] has found that the so-called Einasto profile

$$\rho_{\rm Einasto}(r) = \rho_s \cdot \exp\left[-\frac{2}{\alpha}\left(\left(\frac{r}{r_s}\right)^{\alpha}-1\right)\right], \qquad \alpha = 0.17 \tag{2}$$

MW halo model	r_s in kpc	ρ_s in GeV/cm^3	$\bar{J}$ (10^{-5})
NFW [18]	20	0.26	$15 \cdot 10^3$
Einasto [19]	20	0.06	$7.6 \cdot 10^3$
Isothermal [20]	5	1.16	13

Table 1: Parameters of the density profiles for the Milky Way discussed in the text and corresponding value of $\bar{J}$ for $\Delta\Omega = 10^{-5}$. In all cases we imposed the normalization $\rho(r_\odot) = 0.3$ GeV/cm^3.

should be preferred, since the profiles of simulated halos appeared to become shallower and shallower towards the Galactic center, without converging to a definite power-law. Finally, a truncated isothermal profile

$$\rho_{\rm iso}(r) = \frac{\rho_s}{1 + \left(\frac{r}{r_s}\right)^2} \tag{3}$$

is sometimes adopted as a conservative choice, since it is representative of 'shallow' DM profiles [20]. The Moore [21] density profile is instead somewhat at the other end of the spectrum as it represents the most extreme choice in terms of cuspiness at the Galactic Center.

In Table 1, we show the parameters of the aforementioned density profiles for the case of the Milky Way. Note that, for the Einasto profile, we choose a value of $r_s = 20$ kpc representative of the results of Ref. [19] for different simulations.

The choice of profile introduces an element of astrophysical uncertainty over which to scan.

2.2. Primary spectra at annihilation

We assume that the primary annihilation products contain two SM particles, so that the possible cases are

$$W^+W^-, \quad ZZ, \quad Zh, \quad hh, \qquad e^+e^-, \quad \mu^+\mu^-, \quad \tau^+\tau^-, \qquad b\bar{b}, \quad t\bar{t}, \quad q\bar{q}, \tag{4}$$

where q denotes any light quark, u, d, s, c. In view of the presumed neutrality of the DM particle we have not included final states containing photons.

From these primary two-body states that can be produced in DM annihilations, we next need to produce the spectra of final-state e, p, ν from their decay, hadronization etc. As discussed in [11], these are computed using MonteCarlo codes such as PYTHIA [13], interfaced with custom routines (that allow, among other things, to take into account polarizations). In this way we obtained the e and p spectra plotted in Fig.1.

These spectra will undergo deformations due to the propagation effects of the charged

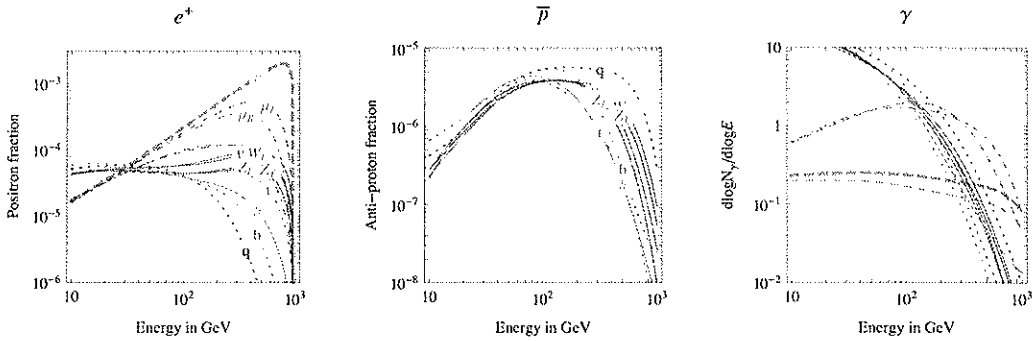

Figure 1: Comparison of the electron (left) and proton (center) fractions and photon (right) fluxes produced by possible DM annihilation channels, for $M = 1$ TeV.

particles in the galactic halo, to be discussed next.

2.3. Positron propagation

The positron flux per unit energy from DM annihilations in any point in space and time is given by $\Phi_{e^+}(t, \vec{x}, E) = v_{e^+} f/4\pi$ (units $1/\text{GeV} \cdot \text{cm}^2 \cdot \text{s} \cdot \text{sr}$) where v_{e^+} is the positron velocity (essentially equal to c in the regimes of our interest) and the positron number density per unit energy, $f(t, \vec{x}, E) = dN_{e^+}/dE$, obeys the diffusion-loss equation:

$$\frac{\partial f}{\partial t} - K(E) \cdot \nabla^2 f - \frac{\partial}{\partial E}\left(b(E) f\right) = Q \tag{5}$$

with diffusion coefficient $K(E) = K_0 (E/\text{GeV})^\delta$ and energy loss coefficient $b(E) = E^2/(\text{GeV} \cdot \tau_E)$ with $\tau_E = 10^{16}\,\text{s}$. They respectively describe transport through the turbulent magnetic fields and energy loss due to synchrotron radiation and inverse Compton scattering on CMB photons and on infrared galactic starlight. Eq.5 is solved in a diffusive region with the shape of a solid flat cylinder that sandwiches the galactic plane, with height $2L$ in the z direction and radius $R = 20\,\text{kpc}$ in the r direction [15]. The location of the solar system corresponds to $\vec{x} = (r_\odot, z_\odot) = (8.5\,\text{kpc}, 0)$. The boundary conditions impose that the positron density f vanishes on the surface of the cylinder, outside of which positrons freely propagate and escape. Values of the propagation parameters δ, K_0 and L are deduced from a variety of cosmic ray data and modelizations. They represent a source of uncertainty over which to scan in order to reach the final predictions for the fluxes. We consider the sets presented in Table 2 [16].

Finally, the source term due to DM DM annihilations in each point of the halo

	Positrons		Antiprotons			
Model	δ	K_0 (kpc^2/Myr)	δ	K_0 (kpc^2/Myr)	$V_{\rm conv}$ (km/s)	L (kpc)
MIN	0.55	0.00595	0.85	0.0016	13.5	1
MED	0.70	0.0112	0.70	0.0112	12	4
MAX	0.46	0.0765	0.46	0.0765	5	15

Table 2: Propagation parameters for charged (anti)particles in the galaxy (from [16] and [17]).

with DM density $\rho(r)$ is

$$Q = \frac{1}{2}\left(\frac{\rho}{M_{\rm DM}}\right)^2 f_{\rm inj}, \qquad f_{\rm inj} = \sum_k \langle\sigma v\rangle_k \frac{dN^k_{e^+}}{dE} \tag{6}$$

where k runs over all the channels with positrons in the final state, with the respective thermal averaged cross sections σv.

The solution for the positron flux at Earth can be written in a useful semi-analytical form [16,22]:

$$\Phi_{e^+}(E,\vec{r}_\odot) = B\frac{v_{e^+}}{4\pi b(E)}\frac{1}{2}\left(\frac{\rho_\odot}{M_{\rm DM}}\right)^2 \int_E^{M_{\rm DM}} dE'\; f_{\rm inj}(E')\cdot I\left(\lambda_D(E,E')\right) \tag{7}$$

where $B \geq 1$ is an overall boost factor discussed below, $\lambda_D(E,E')$ is the diffusion length from energy E' to energy E. The adimensional 'halo function' $I(\lambda_D)$ [16] fully encodes the galactic astrophysics and is independent on the particle physics model. Its possible shapes are plotted in fig.2a for most common choices of DM density profiles and set of positron propagation parameters.

The flux of positrons from DM annihilations has to be summed to the expected astrophysical background. We take the latter from the CR simulations of [24] as parameterized in [25] by $\Phi^{\rm bkg}_{e^+} = 4.5\,E^{0.7}/(1+650\,E^{2.3}+1500\,E^{4.2})$ for positron and $\Phi^{\rm bkg}_{e^-} = \Phi^{\rm bkg,\,prim}_{e^-} + \Phi^{\rm bkg,\,sec}_{e^-} = 0.16\,E^{-1.1}/(1+11\,E^{0.9}+3.2\,E^{2.15}) + 0.70\,E^{0.7}/(1+110\,E^{1.5}+580\,E^{4.2})$ for electrons, with E always in units of GeV. These not-so-recent background computations have recently been revised and questioned [26]: background shapes with a downturn around energies of a few GeV have been investigated in order to incorporate the PAMELA excess as a feature of the background.

2.4. Antiproton propagation

The propagation of anti-protons through the galaxy is described by a diffusion equation analogous to the one for positrons. Again, the number density of anti-protons per unit energy $f(t,\vec{x},T) = dN_{\bar{p}}/dT$ vanishes on the surface of the cylinder at $z = \pm L$ and $r = R$. $T = E - m_p$ is the $\bar{p}$ kinetic energy, conveniently used instead of the total energy E (a distinction which will not be particularly relevant

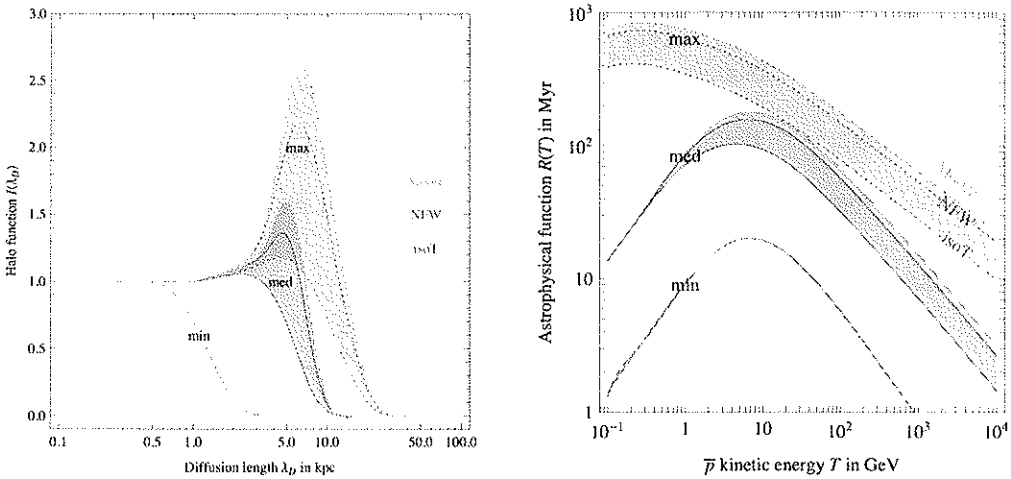

Figure 2: The astrophysical propagation functions for positrons and antiprotons. Left: The 'halo function' $I(\lambda_D)$ of eq.7 that encodes the astrophysics of DM DM annihilations into positrons and their propagation up to the Earth. The diffusion length is related to energy losses as in eq. (14) of [23], that also provides fit functions for all cases. Right: The somewhat analogous $\bar{p}$ astrophysical function $R(T)$ of eq.9. In both cases, the dashed (solid) [dotted] bands assumes the min (med) [max] propagation configuration of table 2. Each band contains 3 lines, that correspond to the isothermal (red lower lines), NFW (blue middle lines) and Moore (green upper lines) DM density profiles.

for our purposes as we look at energies much larger than the proton mass m_p). Since $m_p \gg m_e$ we can neglect the energy loss term, and the diffusion equation for f is

$$\frac{\partial f}{\partial t} - K(T) \cdot \nabla^2 f + \frac{\partial}{\partial z}\left(\mathrm{sign}(z)\, f\, V_{\mathrm{conv}}\right) = Q - 2h\,\delta(z)\,\Gamma_{\mathrm{ann}} f. \tag{8}$$

The pure diffusion term can again be written as $K(T) = K_0 \beta\, (p/\mathrm{GeV})^{\delta}$, where $p = (T^2 + 2m_p T)^{1/2}$ and $\beta = v_{\bar{p}}/c = \left(1 - m_p^2/(T+m_p)^2\right)^{1/2}$ are the antiproton momentum and velocity. The V_{conv} term corresponds to a convective wind, assumed to be constant and directed outward from the galactic plane, that tends to push away $\bar{p}$ with energy $T \lesssim 10\, m_p$. The different sets of values of the parameters are given in table 2. The last term in eq. (8) describes the annihilations of $\bar{p}$ on interstellar protons in the galactic plane (with a thickness of $h = 0.1\,\mathrm{kpc} \ll L$) with rate $\Gamma_{\mathrm{ann}} = (n_{\mathrm{H}} + 4^{2/3} n_{\mathrm{He}}) \sigma_{p\bar{p}}^{\mathrm{ann}} v_{\bar{p}}$, where $n_{\mathrm{H}} \approx 1/\mathrm{cm}^3$ is the hydrogen density, $n_{\mathrm{He}} \approx 0.07\, n_{\mathrm{H}}$ is the Helium density (the factor $4^{2/3}$ accounting for the different geometrical cross section in an effective way) and the $\sigma_{p\bar{p}}^{\mathrm{ann}}$ given esplicitely in [23,27,22]. We neglect the effect of "tertiary anti-protons". This refers to primary $\bar{p}$ after they have undergone non-annihilating interactions on the matter in the galactic disk, losing part of their energy. In this case the solution [28,29,30] for the antiproton flux at the position of the Earth $\Phi_{\bar{p}}(T, \vec{r}_{\odot}) =$

$v_{\bar{p}}/(4\pi)f$ acquires a simple factorized form (see e.g. [17])

$$\Phi_{\bar{p}}(T,\vec{r}_\odot) = B\frac{v_{\bar{p}}}{4\pi}\left(\frac{\rho_\odot}{M_{\rm DM}}\right)^2 R(T)\sum_k \frac{1}{2}\langle\sigma v\rangle_k \frac{dN^k_{\bar{p}}}{dT} \tag{9}$$

where B is the boost factor. The k index runs over all the annihilation channels with anti-protons in the final state, with the respective cross sections; this part contains the particle physics input. The function $R(T)$ encodes all the astrophysics and depends on the choice of halo profile and propagation parameter set. It is plotted in fig.2 for several possible choices. Finally, for completeness we also take into account the solar modulation effect, due to the interactions with the solar wind, that distorts the spectrum via a slight increase of the low energy tail, as described in more detail in [31,23].

The astrophysical background is predicted by the detailed analysis in [32], the results of which we find to be well reproduced by a fitting function of the form $\log_{10}\Phi^{\rm bkg}_{\bar{p}} = -1.64 + 0.07\,\tau - \tau^2 - 0.02\,\tau^3 + 0.028\,\tau^4$ with $\tau = \log_{10}T/{\rm GeV}$. We take for definiteness the flux corresponding to the 'MED' propagation parameters. Particularly favorable is the fact that the uncertainty in the estimates of the background is quite narrow around $10 - 100$ GeV, the most interesting region for current results.

3. Positrons, electrons and antiprotons: which Dark Matter can fit the data?

With the ingredients above, we are ready to address the question "Which characteristics must a Dark Matter candidate have in order to fit the above data?". We first show some illustrative examples (Fig.3) and then proceed to discussing the global fits for all masses and primary annihilation channels (Fig.4).

As a first example, the upper row of Fig.3 shows the spectra of the positron fraction (first column), of the sum of electrons and positrons (second column) and of the antiprotons (third column) from a DM particle with 150 GeV mass and annihilating into W^+W^-. As apparent, the candidate can fit well the positron data, but produces too large a flux of antiprotons: such a Dark Matter is excluded by data with pretty high confidence.

Let us instead consider (third row of Fig.3) a candidate with a (very large) 10 TeV mass, again annihilating into W^+W^-. The positron data points are well fitted (by the low energy tail of the spectrum, in this case) and the antiproton bounds are not exceded, thanks to the fact that an excess would show only at larger energies. However the peak reported by the balloon experiments at around 1 TeV is not reproduced.

As a third exemple, we consider a 1 TeV candidate with annihilations into $\mu^+\mu^-$ (second row of Fig. 3): it fits all the available datasets.

We now proceed to presenting the results of the fits in a more systematic way. In performing such fits, we smoothly scan over the propagation configurations and halo

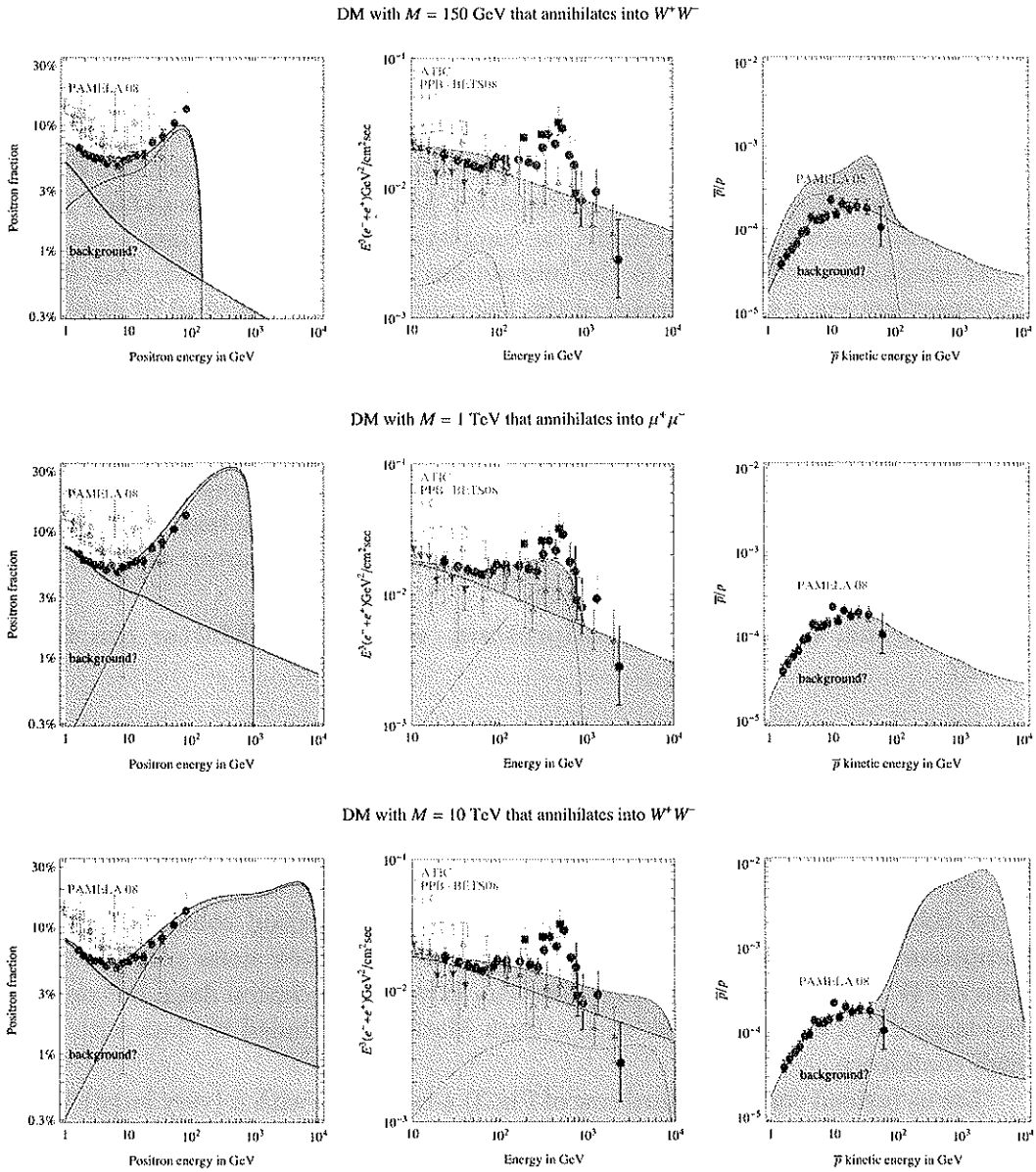

Figure 3: *Three examples of fits of e^+ (left), $e^+ + e^-$ (center), $\bar{p}$ (right) data, for a DM particle with mass $M = 150$ GeV annihilating into W^+W^- (upper row, excluded by $\bar{p}$), $M = 10$ TeV into W^+W^- (lower row, disfavored by the current $e^+ + e^-$ excess), $M = 1$ TeV into $\mu^+\mu^-$ (middle row, favored by data). Galactic DM profiles and propagation models are varied to provide the best fit. See Sec. 3 for the discussion on the treatment of the uncertain astrophysical background.*

models, within the boundaries described above in Sec. 2.3, 2.4 and 2.2. The MED configuration is sometimes considered as favored, but we do not attach a statistical meaning to this sentence. Moreover, we assume that the $e^+, e^-, \bar{p}$ background spectra can be freely renormalized, and have independent ± 0.05 errors in their energy slope (namely, the central values discussed in Sec. 2.3 and 2.4 are multiplied by $A\,E^p$ and the resulting χ^2 is minimized with respect to $p = 0 \pm 0.05$ and to A). This mimics the main uncertainties in astrophysical backgrounds[a], produced by the Fermi mechanism of acceleration, that typically generates power-law spectra (up to some cut-off) but does not predict its coefficient. We will show plots of the χ^2 as a function of the DM mass: an interval at n standard deviations corresponds (in Gaussian approximation) to $\chi^2 < \chi^2_{\rm min} + n^2$, irrespectively of the number of data points. We will not report the value of χ^2/dof as it is a poor statistical indicator; furthermore the number of dof is not a well-defined quantity when (as in the present case) data-points with accuracies much smaller than astrophysical uncertainties are effectively irrelevant.

First, let us consider the fit to PAMELA positron [3] ($e^+/(e^+ + e^-)$) data only (16 data points).
We see in the upper left panel of fig. 4 that DM annihilations into e, μ, τ, W can reasonably well reproduce the data for any DM mass, while annihilations into Z, t, q, b, h give a good fit for DM heavier than about 1 TeV. It is perhaps interesting to note that, contrary to what commonly thought, the spectrum from W^+W^- annihilations is not too flat to give a good fit of the quite steep PAMELA rise. At small masses (see e.g. the upper-left panel of Fig. 3) a MIN configuration of the propagation parameters (and a proper variation of the background curve within the limits considered above) allows to fit the data. At large DM masses (see e.g. the lower-left panel of Fig. 3) the low-x portion of the primary spectrum is steep enough to do the job (as usual, $x = E/M_{\rm DM}$).

Next, let us add the PAMELA $\bar{p}/p$ data [6] (17 data points). Since no excess seems present in the $\bar{p}/p$ ratio, annihilation into leptons are not constrained as they do not produce antiprotons. On the contrary, all other annihilations into quarks, vector and Higgs bosons are significantly constrained, and allowed only if the DM particle is heavier than almost 10 TeV (see the upper left panel of fig. 4). Only in such a case the proton excess lays at energies above those explored currently by PAMELA, while the low energy proton spectrum is consistent with the background (see Fig. 3 for illustration). The bound dominantly comes from high energy data points where the solar modulation is negligible.

The implications of the complementarity of PAMELA $e^+/(e^+ + e^-)$ and $\bar{p}/p$ data on constraining new physics are therefore evident.

We add now to the fit the balloon (ATIC-2 [7], PPB-BETS [8] and EC [9]) data (37

[a]We checked that this procedure reproduces reasonably well the uncertainty bands reported by more detailed analysis, see e.g. Fig.7 of [32] for the case of antiprotons and Fig.4 of [33] for positrons.

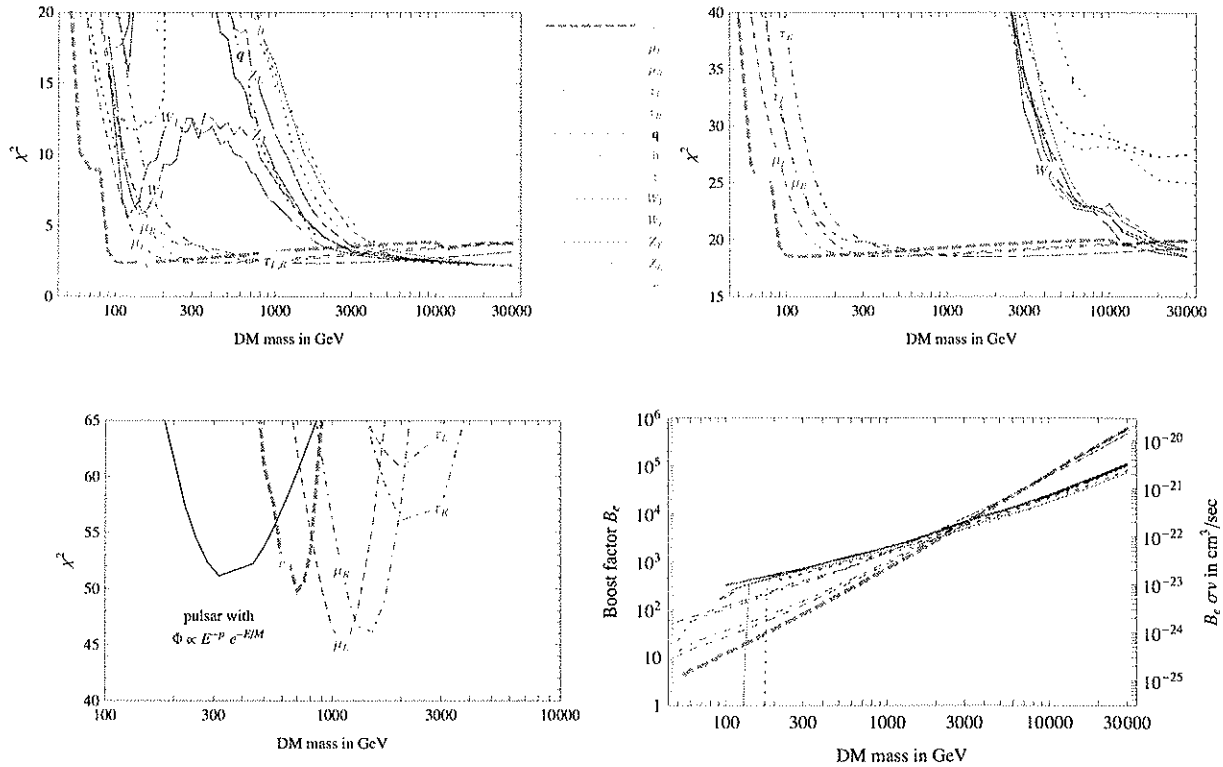

Figure 4: *Global fits of different DM annihilation channels to the data. The labels on each curve indicate the primary annihilation channel. Upper left panel: fit to PAMELA positron fraction data only. Upper right: with the inclusion of PAMELA antiproton data. Lower left: with the inclusion of balloon $e^+ + e^-$ data. Lower right: values of $B_e \cdot \sigma v$ (right axis) and of the boost factor B_e (left axis, for the standard $\sigma v = 3\ 10^{-26}\mathrm{cm}^3/\mathrm{sec}$) needed to fit the data.*

points in total). Because the balloon data shows a sharp cut-off in the excess just below 1 TeV, the DM mass should be close to 1 TeV, and all other but leptonic DM annihilation channels are strongly disfavored or excluded. This is shown in the lower left panel of Fig. 4. More precisely, DM annihilations into μ seem to give the optimal energy spectrum and the best fit (see e.g. the example discussed above in Fig.3). Annihilations into e (τ) give a slightly poorer fit, because of a too (not enough) steep spectrum.

The lower right panel of Fig. 4 illustrates the last important point: the values of the annihilation cross section which are required in order to fit the data (for a given mass and given primary annihilation channel). Values of the order of $10^{-23}\,\mathrm{cm}^3/\mathrm{sec}$ or more (for the masses under consideration) are needed. These are much larger than the typical cross section required by DM thermal production in cosmology

($\sim 3 \cdot 10^{-26}\text{cm}^3/\text{sec}$ [1]). They can be justified in specific models in terms of some enhancement mechanism which is effective today but not in the early universe (such as a resonance [11,34] or Sommerfeld [35,36,11,37] enhancement, the presence of an astrophysical boost factor due to DM substructures –unlikely[38]–, or a combination of these).

4. An astrophysical explanation of the $e^{\pm}$ excesses?

Of course, the origin of the e^+e^- excesses could simply lie in ordinary (albeit possibly peculiar) astrophysical sources, such as one or more pulsars [39], sources of Cosmic Rays in galactic spiral arms [40], aged SuperNova remnants [41] or exploding stars [42]. In this case, the sources would be located in the galactic disk, and moreover not too far from the Earth, since $e^{\pm}$ quickly loose energy when travelling from more that about 1 kpc away.

While I leave all the discussion to the above references, the overall impression is that the astrophysical interpretations are quite viable, but more work is needed to actually be able to predict precisely their detailed features, and in particular to be able to distinguish with certainty a Dark Matter from an astrophysical origin. So these explanations will be confirmed or ruled out by further, more precise measurements of the spectra and possibly improved computations of the expected yields.

5. Constraints from gamma rays and radio observations of the Galactic Center region

Given these tantalizing but surprising hints of Dark Matter annihilations in the charged particle signals, it is now crucial to consider the constraints on this interpretation that come from the photon fluxes that necessarily accompany such charged particles. These photon fluxes are produced:

i) directly as a product of the DM annihilations themselves (mainly from the bremsstrahlung of charged particles and the fragmentation of hadrons, e.g. π^0, produced in the annihilations), at energies comparable to the DM mass M, i.e. in the γ-ray energy range of tens of GeV to multi-TeV.

ii) at much lower energies, e.g. radio to visible frequency, by the synchrotron radiation emitted in the galactic magnetic field by the electrons and positrons produced by DM annihilations.

The best targets to search for these annihilation signals are regions with high DM densities, such as the Milky Way Galactic Center (GC), the Milky Way Galactic Ridge (GR) and the Sagittarius Dwarf spheroidal satellite galaxy (Sgr dSph). The predicted photon fluxes can then be compared with observational data, in order to

rule out combinations of astrophysical and particle physics parameters that violate observational constraints.

5.1. High energy gamma rays

We start by considering the γ-ray fluxes produced by DM annihilations directly. The differential flux of photons from a given angular direction $d\Omega$ is

$$\frac{d\Phi_\gamma}{d\Omega\, dE} = \frac{1}{2}\frac{r_\odot}{4\pi}\frac{\rho_\odot^2}{M_{\rm DM}^2} J \sum_f \langle\sigma v\rangle_f \frac{dN_\gamma^f}{dE}, \qquad J = \int_{\rm line-of-sight} \frac{ds}{r_\odot}\left(\frac{\rho(r)}{\rho_\odot}\right)^2 \tag{10}$$

where the notations are the same as those of the previous Sections. The adimensional quantity J encodes the astrophysical uncertainty. When observing a region with total angular size $\Delta\Omega$ the factor $J\ d\Omega$ gets replaced by $\bar{J}\cdot\Delta\Omega = \int_{\Delta\Omega} J\ d\Omega$. Its values for the Galactic Center region are listed in table 1.

HESS observations in the direction of the Galactic Center have revealed a source of Very High Energy γ-ray emission (HESS J1745-290) lying within $7'' \pm 14''_{\rm stat} \pm 28''_{\rm syst}$ from the supermassive black hole Sgr A*, and compatible with a point source of size less then $1.2'$ [43]. The corresponding energy spectrum is well fitted by a power law $d\Phi_\gamma/dE \propto E^{-2.25\pm0.04}$, over two decades in energy, and it has been confirmed by the MAGIC collaboration [44]. Here, we take a conservative approach and consider the observed gamma-ray emission as an upper limit to the DM annihilation flux, in order to test the compatibility with a DM interpretation of the PAMELA data. We compute the constraints in the σv versus mass plane, by requiring that DM annihilation flux does not exceed (at 3σ, in terms of the error bars quoted by the HESS collaboration) the observed emission *at any data point.*

The HESS collaboration has also recently discovered a diffuse gamma-ray emission, correlated spatially with the Galactic Ridge (GR), a complex of giant molecular clouds in the central 200 pc of the Milky Way [45]. Once point sources, including HESS J1745-290, are subtracted, the reconstructed gamma-ray spectrum for the region with galactic longitude $-0.8° < \ell < 0.8°$ and latitude $|b| < 0.3°$ is well described by a power law with photon index $\Gamma = 2.29 \pm 0.07_{\rm stat} \pm 0.20_{\rm syst}$. In this region, the predicted DM signal is smaller than in a small cone pointing towards the Galactic center, but the astrophysical background is also significantly reduced, and the constraints are less sensitive to the slope of the DM density profile. The same discussion as above for deriving constraints from these observations applies.

In figures 5 and 6 we show the results of the analysis of the data described above. The continuous blue lines shows our conservative bounds on the annihilation cross section σv from HESS observations of the Galactic Center, and the dot-dashed blue lines show the comparable bounds from Galactic Ridge observations. Figs. 5 refer

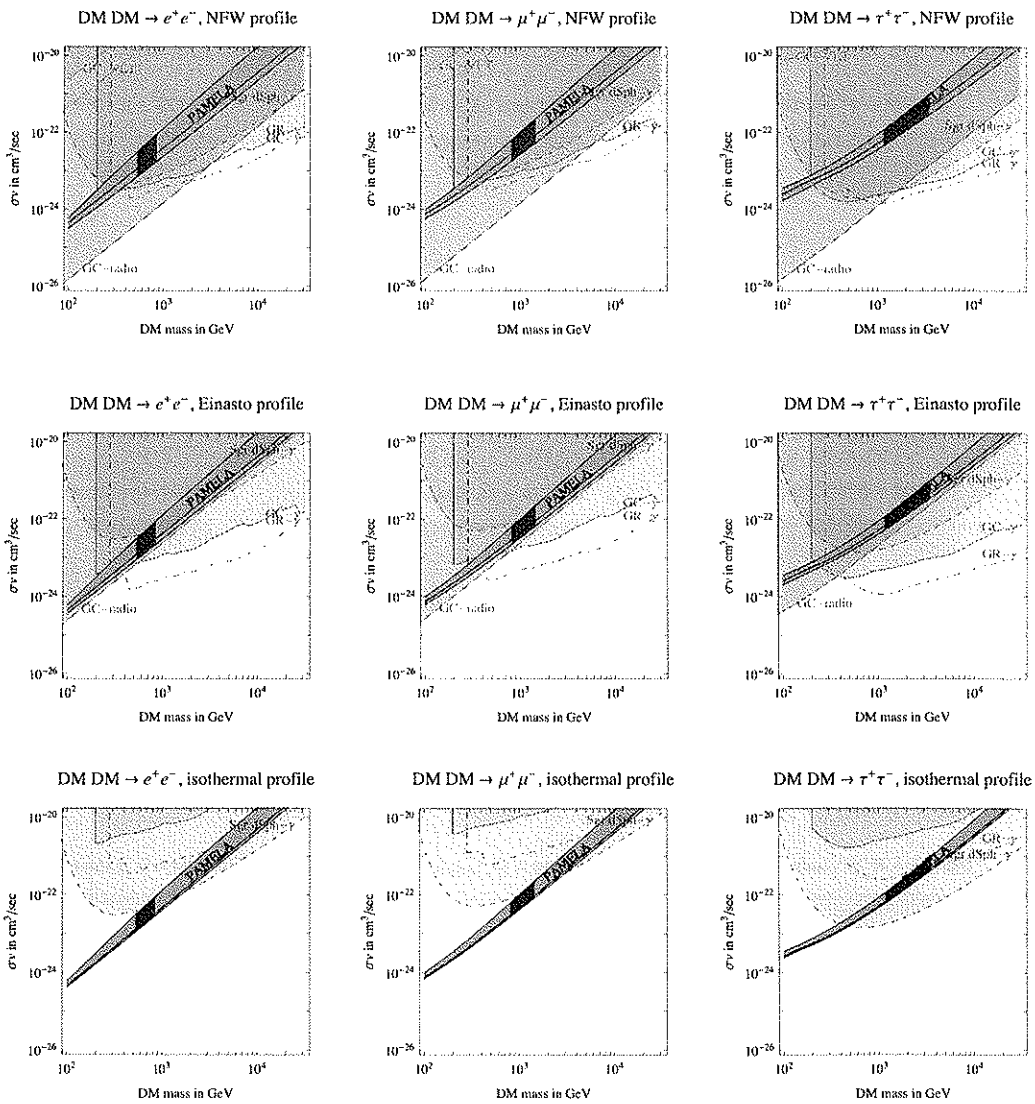

Figure 5: *Comparison of the regions favored by PAMELA (green bands) and ATIC (red regions within the bands) with the bounds from HESS observations of the Galatic Center* [43] *(blue continuous line), Galactic Ridge* [45] *(blue dot-dashed), and SgrDwarf* [46] *(blue dashed) and of observations of the Galactic Center at radio-frequencies* $\nu = 408\,\mathrm{GHz}$ *by Davies et al.* [49] *(red lines) and at* $\nu \sim 10^{14}\,\mathrm{Hz}$ *by VLT* [50] *(upper purple lines, when present, for equipartition and constant magnetic field). We considered DM annihilations into* e^+e^- *(left column),* $\mu^+\mu^-$ *(middle),* $\tau^+\tau^-$ *(right), unity boost and Sommerfeld factors and the NFW (upper row), Einasto (middle), isothermal (lower) MW DM density profiles and the NFW (upper), large core (middle and lower) Sgr dSph DM density profiles.*

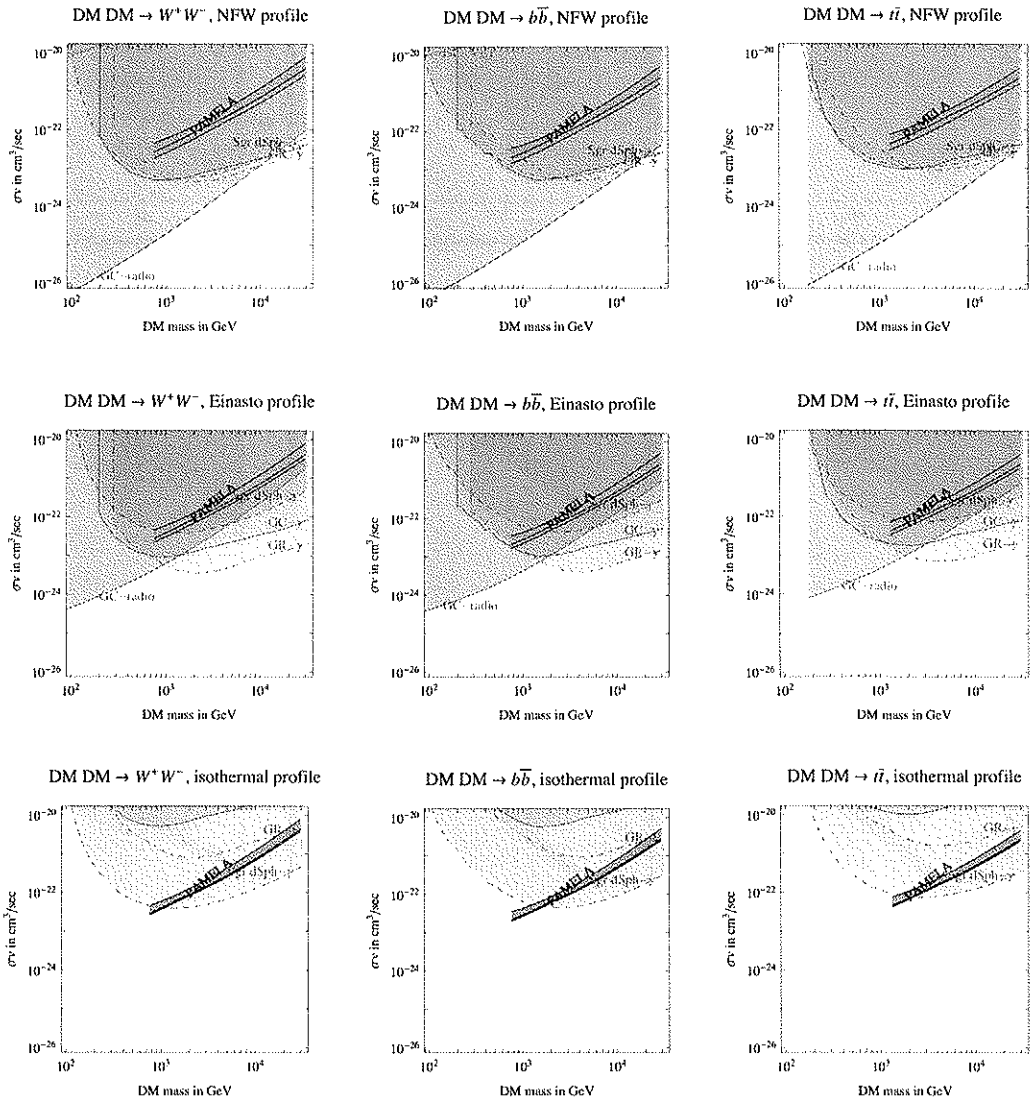

Figure 6: *As in the previous fig.5, but for the cases of DM annihilations into W^+W^- (left), $b\bar{b}$ (middle), $t\bar{t}$ (right).*

Sgr dSph halo	Parameters	Core/Scale radius	$\bar{J}\,(2\cdot 10^{-5})$	$\bar{\mathcal{J}}\,(2\cdot 10^{-5})$
Small core [46]	$v_a = 13.4$ km/s	$r_c = 1.5$ pc	$31\cdot 10^3$	74 10^{24} GeV^2/cm^5
NFW [18]	$\rho_s = 5.2$ GeV/cm^3	$r_s = 0.62$ kpc	$1\cdot 10^3$	2.46 10^{24} GeV^2/cm^5
Large core [47]	$v_a = 22.9$ km/s	$r_c = 0.23$ kpc	$0.14\cdot 10^3$	0.32 10^{24} GeV^2/cm^5

Table 3: *Parameters of the density profiles for the Sagittarius Dwarf galaxy discussed in the text and the corresponding value of $\bar{J}(\Delta\Omega)$ (normalized by convention in terms of the solar quantities $r_\odot$ and $\rho_\odot$, as in eq. (10)) for $\Delta\Omega = 2\cdot 10^{-5}$. For reference, the value of the rescaled $\bar{\mathcal{J}}(\Delta\Omega) = r_\odot \rho_\odot^2\, \bar{J}(\Delta\Omega)$ is also given.*

to DM annihilation into leptons, while fig.s 6 show the more 'traditional' DM annihilation modes into W^+W^-, $b\bar{b}$ and $t\bar{t}$. Barring the possibility of boost factors or Sommerfeld enhancements different for γ and $e^\pm$ observations, we see in fig.s 5 that the green regions that can fit the PAMELA anomaly (and the red regions that can also fit the ATIC anomaly) are excluded for masses $M \gtrsim 300$ GeV, by two orders of magnitude if DM follows the NFW density profile, by an order unity factor if DM follows the Einasto profile, and are allowed if DM follows the isothermal profile (somewhat disfavored, however, by N-body simulations).
In fig.s 6 a similar situation holds. The green PAMELA bands are here truncated because low DM masses do not allow a good fit to the anti-proton data; the truncation is conservatively put at 1 TeV, but masses up to multi-TeV still do not give a good fit, as discussed above.

5.1.1. Sagittarius Dwarf Satellite Galaxy

HESS has also observed the Sagittarius Dwarf galaxy [46], a satellite of the Milky Way which is located at a distance of $d = 24$ kpc from the Sun. Dwarf spheroidal galaxies are among the most DM-dominated structures, so that they allow to search for γ ray signals of DM annihilations with minimal astrophysical backgrounds. In particular, Sagittarius is thought to be in the process of being disrupted by multiple passages through the Milky Way disk, and the fact that it still exists is taken as an indication of the existence of a substantial amount of Dark Matter in it.

The DM density profile in Dwarf Galaxies is uncertain as much as the one in the Milky Way, with which it might have some correlations. For Sgr dSph we consider the possibilities of a cusped NFW profile [46,47] with density given by eq. 1 and of the class of cored profiles

$$\rho_{\rm core}(r) = \frac{v_a^2}{4\pi G_N}\frac{3r_c^2 + r^2}{(r_c^2 + r^2)^2}. \qquad (11)$$

The normalization factors and the characteristic radii are reported in Table 3, where also the corresponding values of $\bar{J}$, defined according to eq. (10), are given. The area of observation corresponds to an aperture angle of 0.14° i.e. to a size of $\Delta\Omega = 2\cdot 10^{-5}$ [46].

HESS has observed Sagittarius Dwarf for $T_{\rm obs} = 11$ h finding no γ-ray excess: the

integrated photon flux is $N_\gamma \lesssim 85$ at 3σ ($N_\gamma < 56$ at 95% CL [46]). Hence an upper bound can be imposed on the annihilation cross section

$$\sigma v < \frac{8\pi}{T_{\rm obs}} \frac{M^2}{r_\odot \rho_\odot^2 \bar{J} \Delta\Omega} \frac{N_\gamma}{\int dE\ A_{\rm eff}(E) \frac{dN_\gamma}{dE}} \tag{12}$$

where the effective area of HESS for observations at $\sim 20°$ (Sgr dSph is located at 14° galactic latitude) $A_{\rm eff}(E) \sim 10^5\,{\rm m}^2$ in the range $E \gtrsim 70$ GeV is taken from [48].

The resulting bounds on σv are shown as dashed blue lines in figures 5 and 6. The top rows of the figures assume a NFW DM density profile in Sgr dSph: the bounds are overall comparable or slightly less powerful than the bounds from the Galactic Center and Ridge. In all the lower rows we use for Sgr dSph a 'large core' profile, which gives the minimum γ flux among the profiles considered in the literature. The bound becomes the most constraining one when the Milky Way profile is taken to be isothermal. We have not explored whether even smoother profiles of Sgr dSph can be designed (compatibly with observations) that can lift such bound.

5.2. Radio waves from the Galactic Center

The $e^\pm$ produced by DM annihilations within the galactic magnetic field radiate synchrotron radiation. The Galactic Center is presumably the best region to search for this effect, because of the large local value of the DM density and magnetic fields. We do not enter here in the details of the necessary astrophysical and particle physics ingredients (see [12] for the complete discussion): we just mention that we compute the synchrotron emission flux S produced by the populations of $e^\pm$ from DM annihilations presented above, neglecting advection and diffusion but scanning different (extremal) assumptions for the galactic magnetic field.

We compare the predicted flux with observations. Since the observed GC microwave spectrum is harder than what DM decays can produce, the dominant bound is obtained considering the observation available at the lowest observed frequency, $\nu = 0.408\,{\rm GHz}$, performed by [49] in a region with full width half maximum of $4''$. The observation found an upper limit to the measured flux $S = (\nu\, dW_{\rm syn}/d\nu)/(4\pi r_\odot^2) < 2\ 10^{-16}\,{\rm erg/cm^2 sec}$, that constraints from above the flux. The resulting bounds are plotted in fig.s 5 and 6 as red lines. What is seen is that this constraint excludes a large portion of the parameter space for NFW and Einasto DM profiles. The constraint extends to low DM masses (where the γ-ray bounds from HESS are not effective). The variation of the magnetic field negligibly affects the bound, because the radio emission is predominantly produced by outer regions.

A subdominant bound (purple lines) comes from the VLT observation [50] at the larger infrared/visible frequency, $\nu = 0.5\ 10^5\,{\rm GHz}$: $S < 3\ 10^{-12}\,{\rm erg/cm^2 sec}$ from

a region with angular size $0.04''$ i.e. $r < 0.0016\,\mathrm{pc}$. It somewhat depends on the magnetic field profile, and it becomes numerically significant only for spiked DM density profiles [51]. Similarly, observations at higher frequencies give possibly strong but not robust bounds [51], that also strongly depend on the possibility of having an intense 'equipartition' magnetic field close to the Milky Way black hole.

6. Conclusions

En lieu of conclusions, let us try to answer the questions raised in the Introduction.

- *Which characteristics must a Dark Matter candidate have in order to fit the above data?*

  a) on the basis of the e^+ and $\bar{p}$ data from PAMELA, the Dark Matter can be:

     a1) a particle that dominantly annihilates into leptons, with no strong preference for the mass, if above a few hundred GeV;

     a2) a particle that annihilates into W, Z or higgses and that has a mass $\gtrsim 10$ TeV.

  b) adding the peak from ATIC-2, a clear indication for the mass emerges: DM has to be a particle with mass ~ 1 TeV that dominantly annihilates into leptons.

  The upcoming results of ATIC-4 [52], PAMELA, or the first data from the Fermi LAT calorimeter [53] can soon check if a peak is really present in the $e^+ + e^-$ spectrum just below 1 TeV: if the peak is there b) is favored and a) is excluded; if instead the peak is not there, then a) is favored and b) excluded. Intermediate situations will require dedicated re-analysis. Models with $M \ll 1$ TeV appear to be already disfavored.

  For what concerns the magnitude of the annihilation cross section, the large flux above the background in the PAMELA and ATIC data indicates a very large σv, of the order of $10^{-23}\mathrm{cm}^3/\mathrm{sec}$ or more (see lower right panel of Fig. 4).

- *What are the constraints from other observations (mainly of photons from the Galactic Center region)?*

  Constraints are imposed by high energy gamma rays (generated directly from the DM annihilation process) from the galactic center region and from satellite galaxies and by synchrotron radiation (generated by $e^\pm$ in the galactic center's magnetic field). The results show that the regions of the parameter space that allow to fit the PAMELA (and ATIC) data are disfavored by about one order of magnitude if a benchmark Einasto or NFW profile is assumed. But choosing a smoother profile and/or assuming that a part of the cross section is due to an

astrophysical boost factor that would not be present in dwarf galaxies and the Galactic Center due to tidal disruption re-allows part of the space.

- *Which conclusions can be drawn on the Dark Matter interpretation of the data?*

  As apparent, the data point to a Dark Matter particle that (1) features really 'unexpected' properties and (2) has anyway disturbing 'internal' tensions (e.g. with γ ray constraints). So, either the DM interpretation is not the right one, i.e. an astrophysical source will turn out to be responsible for the excesses. Or we are on the verge of a big change of paradigm in the field of Dark Matter modelling.

7. Acknowledgements

I would like to warmly thank the organizers of the XIII International Workshop on "Neutrino Telescopes" in Venice for their kind availability and the atmosphere of the meeting. I thank my collaborators Alessandro Strumia, Gianfranco Bertone, Carolin Braüninger, Mario Kadastik, Paolo Panci, Martti Raidal and Marco Taoso for the work presented here. I thank the EU Marie Curie Research & Training network "UniverseNet" (MRTN-CT-2006-035863) for support.

8. References

1) Recent reviews include: G. Jungman, M. Kamionkowski, K. Griest, Phys. Rep., 267, 195, 1996. G. Bertone, D. Hooper and J. Silk, Phys. Rept. 405 (2005) 279 [arXiv:hep-ph/0404175]. J. Einasto, arXiv:0901.0632 [astro-ph.CO].
2) P. Picozza *et al.*, Astropart. Phys. **27** (2007) 296 [arXiv:astro-ph/0608697].
3) O. Adriani *et al.* [PAMELA Collaboration], arXiv:0810.4995.
4) S. W. Barwick *et al.* [HEAT Collaboration], Astrophys. J. 482 (1997) L191 [arXiv:astro-ph/9703192].
5) AMS-01 Collaboration: M. Aguilar et al., Phys. Lett., B646, 145-154, 2007 (astro-ph/0703154).
6) O. Adriani *et al.*, arXiv:0810.4994.
7) ATIC collaboration, Nature 456 (2008) 362.
8) PPB-BETS collaboration, 0809.0760. Web page: `http://ppb.nipr.ac.jp`.
9) T. Kobayashi, J. Nishimura, Y. Komori, T. Shirai, N. Tateyama, T. Taira, K. Yoshida, T. Yuda (EC collaboration), Proceedings of 1999 ICRC, Salt Lake City 1999, Cosmic ray, vol. 3, pag. 61–64.
10) F. Aharonian *et al.* [H.E.S.S. Collaboration], Phys. Rev. Lett. 101 (2008) 261104 [arXiv:0811.3894].

11) M. Cirelli, M. Kadastik, M. Raidal and A. Strumia, Nuclear Physics B 813 (2009), pp. 1-21 [arXiv:0809.2409].
12) G. Bertone, M. Cirelli, A. Strumia and M. Taoso, JCAP03 (2009) 009 [arXiv:0811.3744].
13) T. Sjostrand, S. Mrenna, P. Skands, Comput. Phys. Com. 178, 852 (2008) [arXiv:0710.3820].
14) Z. Was and P. Golonka, Nucl. Phys. Proc. Suppl. 144, 88 (2005) [arXiv:hep-ph/0411377].
15) The now standard "two-zone diffusion model" introduced in V.L. Ginzburg, Ya.M. Khazan, V.S. Ptuskin, Astrophysics and Space Science, 68, 295-314, 1980, W.R. Webber, M.A. Lee, M. Gupta, Astrophysical Journal, 390, 96-104, 1992.
16) T. Delahaye, R. Lineros, F. Donato, N. Fornengo and P. Salati, Phys. Rev. D 77 (2008) 063527 [arXiv:0712.2312].
17) F. Donato, N. Fornengo, D. Maurin and P. Salati, Phys. Rev., D 69, 063501, 2004 [astro-ph/0306207].
18) J. Navarro, C. Frenk, S. White, Astrophys. J., 490, 493, 1997 [astro-ph/9611107].
19) A. W. Graham, D. Merritt, B. Moore, J. Diemand and B. Terzic, Astron. J. 132 (2006) 2685 [arXiv:astro-ph/0509417]. J. F. Navarro *et al.* [0810.1522].
20) J. N. Bahcall and R. M. Soneira, Astrophys. J. Suppl., 44, 73, 1980.
21) J. Diemand, B. Moore and J. Stadel, Mon. Not. Roy. Astron. Soc., 353, 624, 2004 [astro-ph/0402267].
22) J. Hisano, S. Matsumoto, O. Saito, M. Senami, Phys. Rev., D73, 055004, 2006 [hep-ph/0511118].
23) M. Cirelli, R. Franceschini and A. Strumia, Nucl. Phys. B 800 (2008) 204 [arXiv:0802.3378].
24) I. V. Moskalenko and A. W. Strong, Astrophys. J., 493, 694, 1998 [astro-ph/9710124].
25) E. A. Baltz and J. Edsjo, Phys. Rev., D59, 023511, 1999 [astro-ph/9808243].
26) T. Delahaye, F. Donato, N. Fornengo, J. Lavalle, R. Lineros, P. Salati and R. Taillet, arXiv:0809.5268.
27) L. C. Tan and L. K. Ng, J. Phys., G 9, 227, 1983.
28) P. Chardonnet, G. Mignola, P. Salati and R. Taillet, Phys. Lett., B 384, 161, 1996 [astro-ph/9606174]. A. Bottino, F. Donato, N. Fornengo and P. Salati, Phys. Rev., D 58, 123503, 1998 [astro-ph/9804137]. See also: L. Bergstrom, J. Edsjo and P. Ullio, Astrophys. J., 526, 215, 1999 [astro-ph/9902012].
29) D. Maurin, R. Taillet, F. Donato, P. Salati, A. Barrau and G. Boudoul [astro-ph/0212111].
30) D. Maurin, F. Donato, R. Taillet and P. Salati, Astrophys. J., 555, 585, 2001 [astro-ph/0101231].

31) L.J. Gleeson and W.I. Axford, ApJ, 149, L115, 1967 and L.J. Gleeson and W.I. Axford, ApJ, 154, 1011, 1968.
32) T. Bringmann and P. Salati, Phys. Rev., D 75, 083006, 2007 [astro-ph/0612514].
33) T. Delahaye et al. [0809.5268]. Lecture by P. Salati at the Cargese 2007 Summer School and talk by N. Fornengo at the NOW 2008 workshop.
34) D. Feldman, Z. Liu and P. Nath, Phys. Rev. D **79** (2009) 063509 [arXiv:0810.5762 [hep-ph]]. M. Ibe, H. Murayama and T. T. Yanagida, arXiv:0812.0072 [hep-ph]. W. L. Guo and Y. L. Wu, Phys. Rev. D **79** (2009) 055012 [arXiv:0901.1450 [hep-ph]].
35) A. Sommerfeld, "Über die Beugung und Bremsung der Elektronen", Ann. Phys. 403, 257 (1931). J. Hisano, S. Matsumoto and M. M. Nojiri, Phys. Rev. Lett. 92 (2004) 031303 [hep-ph/0307216]. J. Hisano, S. Matsumoto, M. M. Nojiri and O. Saito, Phys. Rev. D 71 (2005) 015007 [hep-ph/0407168]. See also previous work in K. Belotsky, D. Fargion, M. Khlopov and R. V. Konoplich, Phys. Atom. Nucl. 71 (2008) 147 [arXiv:hep-ph/0411093] and references therein.
36) M. Cirelli, A. Strumia, M. Tamburini, Nucl. Phys. B **787** (2007) 152 [arXiv:0706.4071 [hep-ph]].
37) N. Arkani-Hamed, D. P. Finkbeiner, T. R. Slatyer and N. Weiner, Phys. Rev. D **79** (2009) 015014 [arXiv:0810.0713 [hep-ph]].
38) See, for a recent analysis, J. Lavalle, J. Pochon, P. Salati and R. Taillet [astro-ph/0603796] and J. Lavalle, Q. Yuan, D. Maurin and X. J. Bi [0709.3634].
39) A. M. Atoian, F. A. Aharonian and H. J. Volk, Phys. Rev. D 52 (1995) 3265. I. Büshing et al. [0804.0220]. T. Kobayashi, Y. Komori, K. Yoshida and J. Nishimura, Astrophys. J. 601 (2004) 340 [astro-ph/0308470]. See also the recent study in: D. Hooper, P. Blasi and P. D. Serpico, arXiv:0810.1527. H. Yuksel, M. D. Kistler and T. Stanev, arXiv:0810.2784 [astro-ph]. S. Profumo, arXiv:0812.4457 [astro-ph]. N. Kawanaka, K. Ioka and M. M. Nojiri, arXiv:0903.3782 [astro-ph.HE]. See also P. D. Serpico, arXiv:0810.4846 for an agnostic analysis.
40) N. J. Shaviv, E. Nakar and T. Piran, arXiv:0902.0376 [astro-ph.HE].
41) P. Blasi, arXiv:0903.2794 [astro-ph.HE]. See also P. Blasi and P. D. Serpico, arXiv:0904.0871. and S. Dado and A. Dar, arXiv:0903.0165 [astro-ph.HE].
42) P. L. Biermann, J. K. Becker, A. Meli, W. Rhode, E. S. Seo and T. Stanev, arXiv:0903.4048 [astro-ph.HE].
43) F. Aharonian *et al.* [The HESS collaboration], Astron. Astrophys. 425 (2004) L13 [astro-ph/0408145]. F. Aharonian *et al.* [HESS collaboration], Phys. Rev. Lett. 97 (2006) 221102 [Erratum-ibid. 97 (2006) 249901] [astro-ph/0610509].
44) J. Albert *et al.* [MAGIC Collaboration], Astrophys. J. 638 (2006) L101 [astro-ph/0512469].

45) F. Aharonian *et al.* [HESS collaboration], Nature 439 (2006) 695 [astro-ph/0603021].
46) HESS collaboration, Astropart. Phys. 29 (2008) 55 [arXiv:0711.2369].
47) N. W. Evans, F. Ferrer and S. Sarkar, Phys. Rev. D 69 (2004) 123501 [astro-ph/0311145].
48) F. Aharonian *et al.* [H.E.S.S. Collaboration], Astron. Astrophys. 457 (2006) 899 [arXiv:astro-ph/0607333].
49) R.D.Davis, D.Walsh, R.S.Booth, MNRAS 177, 319-333 (1976)
50) R. Genzel *et al.*, Nature 425 (2003) 934 [astro-ph/0310821].
51) M. Regis and P. Ullio, Phys. Rev. D 78, 043505 (2008) [arXiv:0802.0234].
52) Talk by J.P. Wefel at ISCRA 2008, Erice, Italy, 2008, `http://laspace.lsu.edu/ISCRA/ISCRA2008`.
53) GLAST collaboration, '*Measuring 10-1000 GeV Cosmic Ray Electrons with GLAST/LAT*', talk at the ICRC07 conference.